SAND 94-2478C

Conf-950167--1

Heterostructures and Infrared Emitters with Compressed InAsSb Layers (Invited)

Steven R. Kurtz and Robert M. Biefeld
Sandia National Laboratories, Albuquerque, NM 87185

Abstract: An overview is presented of strained InAsSb heterostructures and infrared emitters. InAsSb/InGaAs strained-layer superlattices (SLS) and InAsSb quantum wells were characterized using magneto-photoluminescence and compared with unstrained InAsSb and InAs alloys. In heterostructures with biaxially compressed InAsSb, large quantum confinement energies were observed, and the holes exhibited a decrease in effective mass, approaching that of the electrons. This study demonstrates that the electrons and holes in the InAsSb heterostructures are confined in the InAsSb layers, and the band offsets are type I. A large increase in the Auger-1 threshold energy should accompany the strain-induced change in valence-band symmetry of the InAsSb layers. Correspondingly, the InAsSb heterostructures display high radiative efficiencies and increased activation energies for nonradiative recombination compared with the unstrained alloys. LEDs and lasers with InAsSb heterostructure active regions are described. InAsSb/InGaAs SLS LEDs operating at 300K at wavelengths ≤ 5 μm have been demonstrated. Optically pumped InAsSb/InGaAs SLS lasers, with InPSb cladding, had a maximum operating temperature of 100K.

1. Introduction

Frequently, the Auger-1 process (i.e. An electron and hole recombine by scattering a second electron up into the conduction band.) dominates radiative recombination in narrow bandgap III-V semiconductors, and as a result, the wavelength of diode lasers operating at room temperature has been limited to ≤ 2.1-2.3 μm.[1] In a biaxially compressed III-V layer, the |3/2,±3/2> hole ground state can increase the in-plane, electron-hole effective mass ratio (m^*_e/m^*_h) over that found in bulk material. In the 2-dimensional limit, this effective mass ratio will result in an increased threshold energy for Auger-1.[2-4] Therefore, midwave infrared (2-6 μm) emitters with biaxially compressed, InAsSb active regions may exhibit improved performance and higher temperature operation.[5] In this paper, we will describe the optical characterization of InAsSb/InGaAs strained-layer superlattices (SLSs) and InAsSb quantum wells with InAs barriers. We determine the electronic properties of these heterostructures and present evidence indicating that a large increase in Auger-1 threshold energy results from the strain-induced valence-band symmetry of the InAsSb layer. LEDs and lasers with InAsSb heterostructure active regions are described.

2. Optical Studies

A. Experimental Details

InAsSb and InGaAs alloys and heterostructures were grown by metal-organic chemical vapor deposition (MOCVD) on InAs substrates. SLS and ternary compositions, layer thicknesses, and lattice constants were determined from both (004) and (115) or (335) x-ray rocking curves. In this study, photoluminescence spectra for an InAsSb/InGaAs SLS and InAsSb quantum wells with InAs barriers are compared with those for unstrained $InAs_{0.93}Sb_{0.07}$ and InAs alloys. The SLS characterized in the optical study was an $InAs_{0.91}Sb_{0.09}$ / $In_{0.87}Ga_{0.13}As$ SLS (90 Å/ 130 Å layer thicknesses), nominally lattice matched to the InAs substrate. The multiple quantum well sample consisted of 318, 159, 106, and 53 Å thick quantum wells of $InAs_{0.91}Sb_{0.09}$, separated by 500 Å thick, InAs barriers. The sum of the four quantum well thicknesses is less than the critical layer thickness (≈ 1000 Å), and the quantum wells are pseudomorphic.

Throughout our studies of As-rich, InAsSb (5-50% Sb), the bandgaps of our InAsSb alloys were smaller than accepted values [6], and the unexpectedly low photoluminescence energies of As-rich, InAsSb heterostructures is traceable to the bandgap

DISCLAIMER

anomaly observed for the InAsSb alloys. Electron diffraction results indicate compositional ordering and phase separation may occur in the As-rich, InAsSb grown at low temperatures by vapor phase epitaxy.[7] As demonstrated in the following discussion, the InAsSb material displays "single phase, random-alloy-like" optical properties except for the bandgap anomaly, and we assume that the strain imposed by the InAs heterostructure dominates any internal strain occurring within domains of the InAsSb.

Midwave infrared photoluminescence was measured by operating an FTIR spectrometer in a double-modulation mode. In the magneto-photoluminescence experiments, a fluoride optical fiber was used to transmit infrared light in the magnet cryostat. The photoluminescent light was collected by the fiber and analyzed with the FTIR equipped with an InSb photodiode. All measurements were made in the Faraday configuration with the magnetic field parallel to the growth, (001), direction of the sample.

B. Magneto-Photoluminescence

Low temperature, zero-field photoluminescence spectra for the multiple quantum well, SLS, unstrained InAsSb, and InAs samples are shown in Figure 1. For each sample, the photoluminescence spectra consists of a single peak with a linewidth of approximately 10 meV. Emission from single quantum wells is clearly resolved in Fig 1(c), with the quantum well thickness indicated in the figure. (InAs barriers, 500 Å thick, separate the quantum wells in Fig. 1(c).) The photoluminescence energies of the thick (318 Å) quantum well and the InAsSb alloy provide estimates of the bandgap energies of the MOCVD alloys, and both alloys exhibit the bandgap anomaly. A large quantum size shift is observed for the quantum wells. Analysis of quantum size effects for InAsSb/InGaAs and InAsSb/InAs heterostructures indicates that both have type I band offsets. Contrary to our experimental results, a type II band offset would result in negligible quantum size shifts for the InAsSb/InAs heterostructure with equal InAs barrier thicknesses. The bandgap and conduction band offset are sensitive to ordering or phase separation occurring in the InAsSb; the valence band offset is insensitive to these effects.

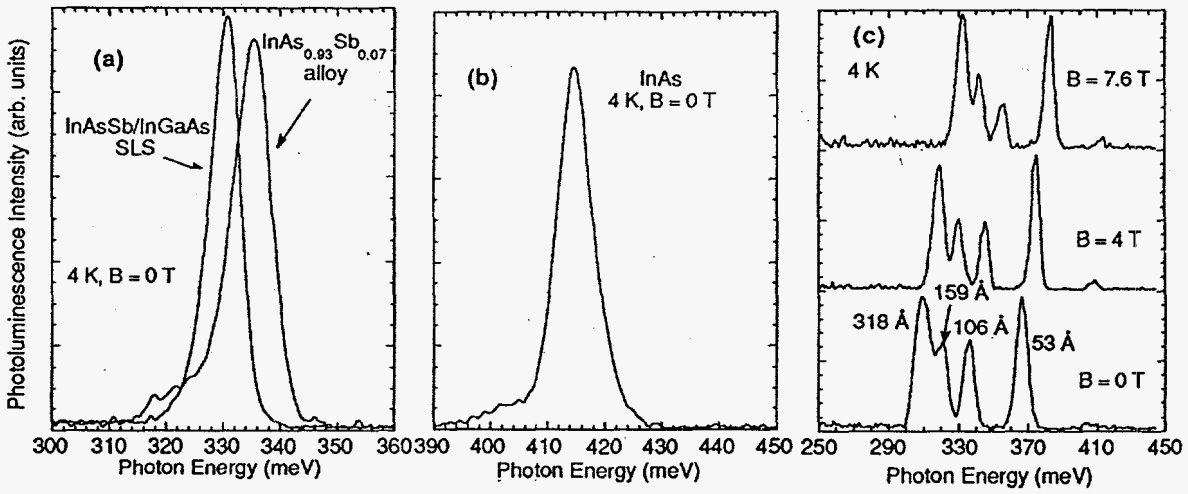

Figure 1 - Photoluminescence spectra of (a) $InAs_{0.91}Sb_{0.09}$ / $In_{0.87}Ga_{0.13}As$ SLS and $InAs_{0.93}Sb_{0.07}$ alloy, (b) InAs, and (c) $InAs_{0.91}Sb_{0.09}$/InAs quantum wells.

The magnetic field dependence of the photoluminescence energies for each of these samples is shown in Figure 2. For each photoluminescence line, the reduced mass, μ, corresponding to the slope obtained from the free electron-hole approximation

$\left(\frac{dE}{dB} = \mu_B\left(\frac{1}{m_e^*} + \frac{1}{m_h^*}\right) = \frac{\mu_B}{\mu}\right.$; μ_B is the Bohr magneton), is indicated in the figure. The reduced masses for the unstrained alloys (μ_{InAsSb}= 0.037 and μ_{InAs}=0.031, in units of free

electron mass) are significantly larger than those observed in the strained heterostructures (μ=0.015-0.024) due to the low in-plane hole mass associated with the heavy-hole (|3/2,±3/2>) ground state of the biaxially compressed, InAsSb layers.

Excitonic behavior is revealed in the magneto-photoluminescence results. For all samples, the photoluminescence peak energy is insensitive to magnetic field for B< 2T, characteristic of a diamagnetic exciton, and in the linear region observed at higher fields, the reduced mass values obtained from the free carrier approximation are consistently too large, due in part to the binding energy of the exciton. Also, note the increase in reduced mass (or decrease in slope) as the quantum wells become thinner (Fig. 2(b)).

Using measured parameters for InAs and semi-empirical expressions for nonparabolicity and magneto-exciton energies, we can estimate exciton binding energies and correct the reduced mass values.[8] Assuming a 3-dimensional exciton, we obtain corrected reduced mass values, μ=0.010, 0.026, and 0.023, for the 318 Å thick quantum well, unstrained InAsSb alloy, and InAs, respectively. The exciton binding energies for the 318 Å well and the alloys were 1.0 meV and 1.8 meV, respectively. Examining the thinnest (53 Å) quantum well, we estimate an exciton binding energy of 2.5 meV for a reduced mass, μ=0.016, and assuming a 3-dimensional exciton. The change in slope in Fig 2(b), associated with quantum confinement, indicates an increase in exciton binding energy of the correct magnitude.[8]

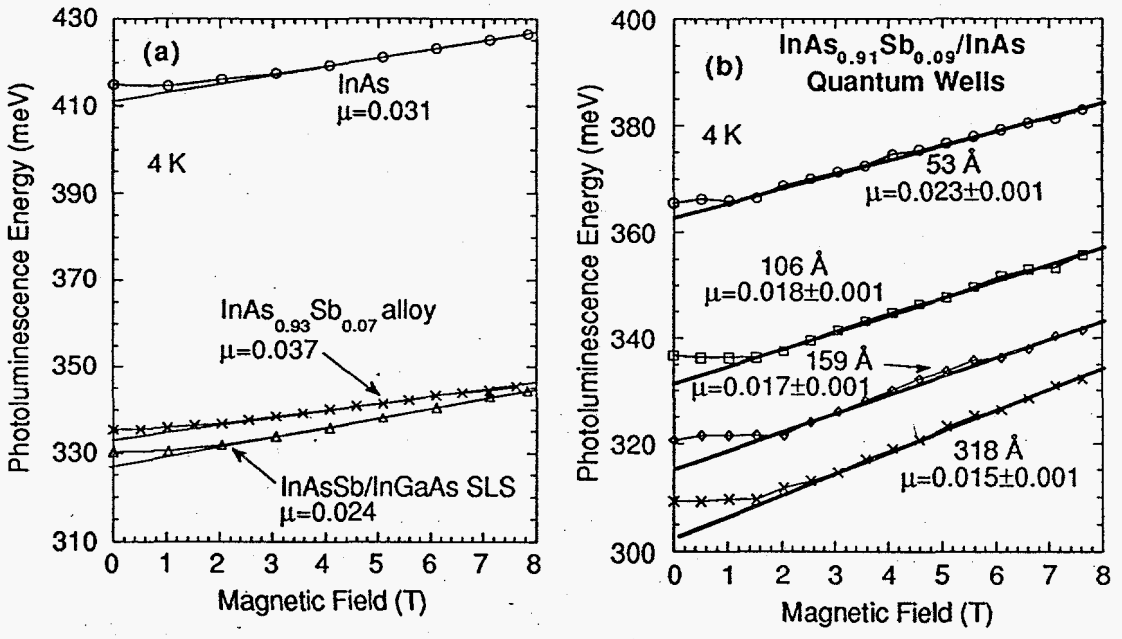

Figure 2 - Magnetic field-induced shift of the photoluminescence energy for (a) the InAsSb/InGaAs SLS and the InAsSb and InAs alloys, and (b) the InAsSb/InAs quantum wells.

C. Modification of Auger-1 Threshold Energies

In the 2-dimensional limit, a large increase in the Auger-1 threshold energy accompanies this strain-induced change in valence-band symmetry. We examined the temperature dependence of the photoluminescence intensity for SLS and bulk, $InAs_{0.93}Sb_{0.07}$ and InAs samples. (see Figure 3) At > 100 K, the radiative efficiency decreases exponentially for all samples, and the activation energy for nonradiative recombination (ΔE) in the SLS displayed a marked increase compared with that of the unstrained alloys (ΔE=0.26 E_{gap} vs ΔE=0.06 E_{gap}). Other InAsSb/InGaAs SLSs that we examined also displayed large activation energies. Due to variations in optical alignment and sample doping and defects, the differences in the relative radiative efficiency between samples may not be accurate, but generally, the SLSs have higher radiative efficiencies than the unstrained alloys.

Approaching room temperature, Auger-1 will be the dominant nonradiative process. The radiative efficiency for extrinsic, n-type material is

$$\eta = \frac{\tau_A}{\tau_R} \propto (1/n_0) \cdot \exp\left(\frac{\Delta E}{kT}\right) \quad (1) \qquad \text{and} \qquad \Delta E = \left(\frac{m_e^*/m_h^*}{1+(m_e^*/m_h^*)}\right) \cdot E_{gap} \quad (2),$$

where n_0 is the electron density, $\tau_R \propto (T/n_0)$ is the radiative lifetime, and $\tau_A \propto (T/n_0^2)\exp(\Delta E/kT)$ is the Auger-1 lifetime (in 2 dimensions).[9] Eq. 1 is based on simple energy-momentum conservation for isotropic, parabolic bands, and the expression for activation energy, ΔE (ΔE = Auger threshold - Bandgap), is valid in 2 or 3-dimensions.[2] In the 2-dimensional limit, the SLS in-plane effective masses determine ΔE,[3,4] and therefore, the SLS activation energy is larger than that of the unstrained alloys due to the decreased hole mass in biaxially compressed layers of the SLS.

Electron-hole effective mass ratios for each sample are compared with theoretical values obtained from k·p calculations and with experimental values obtained from magneto-photoluminescence and temperature dependence studies. In each case there is good agreement between theoretical and experimentally determined mass ratios. The effective mass ratios (m^*_e / m^*_h) determined by the 3 methods for the SLS were in the range, 0.3-0.5 , and the effective mass ratios for the unstrained alloys were 0.06±0.02.[9] Comparing the SLS with the alloys, the SLS consistently displayed the predicted effects of the valence band under biaxial compression.

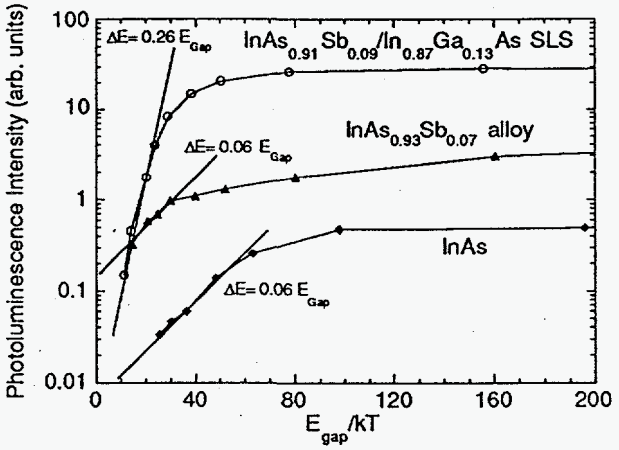

Figure 3 - Temperature dependence of the photoluminescence intensity (radiative efficiency) for the InAsSb/InGaAs SLS and InAsSb and InAs alloys. Activation energies (ΔE) are indicated in the figure.

3. Midwave (4 μm) Emitters

A. Broadband LEDs

For many chemical sensing applications, a broadband LED infrared source is preferred over a diode laser. We have constructed several MOCVD grown, LEDs as infrared sources and laser precursors. These devices demonstrate n and p-type doping of both InAsSb heterostructure and InPSb cladding materials. The LEDs were 380 μm diameter mesa devices with $InAs_{1-x}Sb_x$ / $In_{1-x}Ga_xAs$ SLS (x≈0.1) active regions. Typically, LED and laser emission occurs at the active region photoluminescence energy, shifted to slightly higher energy (≈ 10 meV) by band filling. In devices where the active region and cladding lattice constants are well matched to that of the substrate, defect-related nonradiative recombination is minimized, and the temperature dependence of the LED emission (Fig. 4(a)) resembles the temperature dependence of the SLS radiative efficiency (see Fig. 3). The LED in Figure 4(a) had a low temperature external efficiency of 0.06% at a wavelength, 3.6 μm. Correcting for reflection losses, the internal efficiency may be as high as 2%. As shown in Figure 4(b), these devices operate at room temperature and span the 4-5 μm range necessary

for CO and CO_2 detection. The total external power output of this device at 300 K was 180 nW with 100 mA drive current.[5]

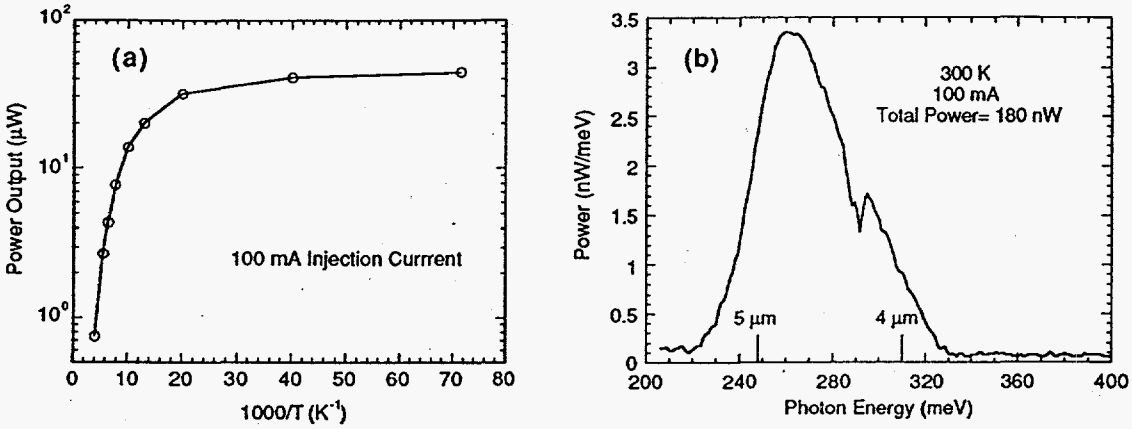

Figure 4 - (a) Temperature dependence of the power output for an InAsSb/InGaAs SLS LED. (b) LED emission spectrum at 300K.

B. Lasers

A laser structure was realized by growing a 2 μm thick layer of $InP_{0.65}Sb_{0.35}$, followed by a 1.5 μm thick SLS active region, on an InAs substrate. Finally, a 100 Å thick InPSb cap layer was grown on top of the SLS to reduce surface recombination. The structure of the active region determined by x-ray analysis was $InAs_{0.87}Sb_{0.13}$ / $In_{0.93}Ga_{0.07}As$ (95 Å/ 133 Å layer thicknesses). The buried InPSb layer and the space

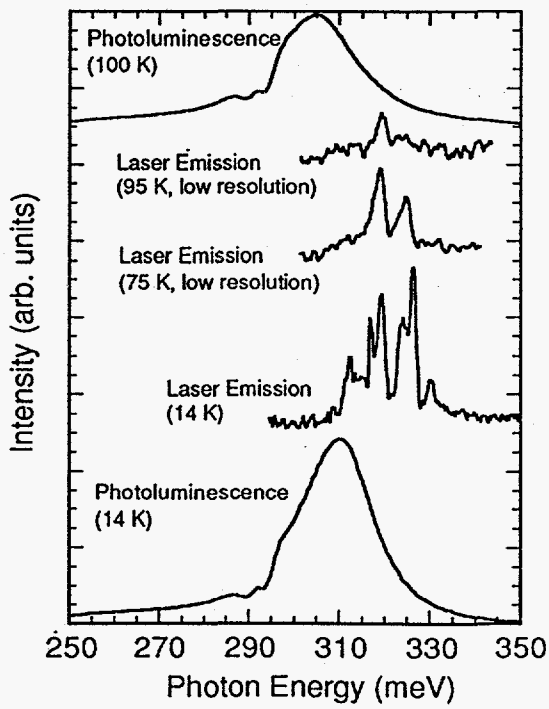

Figure 5 - Photoluminescence and lasing spectra for a SLS/InPSb "single heterostructure" up to 100 K.

above the SLS produced optical confinement within the active region. Laser emission at 3.9 μm was observed by optical pumping cleaved bars. Laser and photoluminescence spectra for the SLS-InPSb structure are shown in Figure 5. The maximum lasing temperature was 100

K.[5] To date, we have not demonstrated electrically injected MOCVD grown, SLS lasers with InPSb claddings operating at ≥ 4 μm. Shorter wavelength, 3.06 μm, electrically injected InGaAsSb/InPSb double heterostructure lasers were marginal and had a maximum operating temperature of 35 K.[10] MBE-grown, electrically injected lasers with InAsSb/InAlAs SLS active regions and AlAsSb claddings have been demonstrated with pulsed operating temperatures up to 85 K.[11] "More work is needed to prove that the strained quantum well structure improves 4 μm laser performance."

4. Conclusions

Using infrared photoluminescence and magneto-photoluminescence, we have examined the electronic properties of a series of heterostructures with biaxially compressed InAsSb. Quantum size studies show that electrons are confined to the InAsSb layer, and magnetic field studies demonstrate that holes are confined to the heavy hole (small in-plane effective mass) ground state of the biaxially compressed InAsSb layers. The band offsets for these heterostructure are type I. Analysis of the magneto-excitonic behavior indicates that the hole mass may be quite small (μ=0.010), and exciton binding energy increases with quantum confinement. The photoluminescence efficiency versus temperature revealed that an increased activation energy for nonradiative recombination accompanies the decreased hole mass in the SLS. Photoluminescence efficiency activation energies for the SLS and unstrained alloys agree with estimated Auger-1 threshold energies, with the activation energy for the SLS approaching the Auger-1 value in the 2-dimensional limit. Although the material properties of the MOCVD-grown InAsSb are non-ideal, these heterostructures display Auger-1 threshold energies, effective masses, band offsets, and "random alloy-like" properties that are desirable for active regions in midwave infrared diode lasers.

Infrared emitters were constructed with MOCVD-grown, compressed InAsSb active regions. InAsSb/InGaAs SLS LEDs may have internal efficiencies as high as 2% at low temperature. Without device modifications to minimize ohmic heating or reflection loss, these LEDs emit ≈ 200 nW over the 4-5 μm range at room temperature. Optically pumped, InAsSb/InGaAs SLS lasers have been demonstrated with a maximum operating temperature of 100 K. Although strained heterostructures hold the promise of reduced Auger-1 rates, 4 μm lasers with these active regions have not yet demonstrated improved performance over lasers with unstrained bulk active regions.

The work presented in this overview resulted from collaborations and conversations with Sandia colleagues; L. R. Dawson, A. J. Howard, M. H. Crawford, D. M. Follstaedt, H. J. Hjalmarson, J. S. Nelson, K. C. Baucom, S. K. Lyo, and E. D. Jones. Further details may be found in their contributions to these proceedings. This work was performed at Sandia National Laboratories, supported by the U. S. Department of Energy under contract No. DE-AC04-94AL85000.

References

[1] Eglash S J and Choi H K 1990 Appl. Phys. Lett. **57** 1292; 1992 Appl. Phys. Lett. **61** 1154.
[2] Dutta N K 1983 J. Appl. Phys. **54** 1236
[3] Adams A R 1986 Elect. Lett. **22** 249
[4] Yablonovich E and Kane E O 1988 IEEE J. Lightwave Tech. **6** 1292
[5] Kurtz S R, Biefeld R M, Dawson L R, Baucom K C, and Howard A J 1994 Appl. Phys. Lett. **64** 812
[6] Fang Z M, Ma K Y, Jaw D H, Cohen R M, and Stringfellow G B 1990 J. Appl. Phys. **67** 7034, and references therein.
[7] Follstaedt D M, Biefeld R M, Baucom K C, and Kurtz S R (accepted for publication, J. Elect. Mat.)
[8] Kurtz S R and Biefeld R M (accepted for publication, Appl. Phys. Lett.)
[9] Kurtz S R, Biefeld R M, and Dawson L R (accepted for publication, Phys. Rev. B)
[10] Menna R J, Capewell D R, Martinelli R U, York P K, and Enstrom R E 1991 Appl. Phys. Lett. **59** 2127.
[11] Choi H K, Turner G W, and Le H Q (to be published).